Textile & Leather Review

ISSN 2623-6281 | www.tlr-journal.com | 10.31881/TLR

Removal of Commercial Textile Dye DRMD from Wastewater Using Two-Dimensional Mesoporous Graphene Oxide Adsorbent

Sadit Bihongo Malitha, Dewan Md. Mahmudunnabi, Mahjabin Rahman Ria, Khandker Saadat Hossain, Md. Abu Sayid Mia, Md. Zahangir Alam

How to cite: Malitha SB, Mahmudunnabi DM, Rahman Ria M, Hossain KS, Sayid Mia MA, Alam MZ. Removal of Commercial Textile Dye DRMD from Wastewater Using Two-Dimensional Mesoporous Graphene Oxide Adsorbent. Textile & Leather Review. 2024; 7:616-643. https://doi.org/10.31881/TLR.2024.039

How to link: https://doi.org/10.31881/TLR.2024.039

Published: 26 April 2024

Removal of Commercial Textile Dye DRMD from Wastewater Using Two-Dimensional Mesoporous Graphene Oxide Adsorbent

Sadit Bihongo MALITHA[1], Dewan Md. MAHMUDUNNABI[1], Mahjabin RAHMAN RIA[1], Khandker Saadat HOSSAIN[2], Md. Abu SAYID MIA [1,4], Md. Zahangir ALAM[1,3]*

[1]Department of Applied Chemistry and Chemical Engineering, University of Dhaka, Dhaka 1000, Bangladesh

[2]Department of Physics, University of Dhaka, Dhaka 1000, Bangladesh

[3]Atish Dipankar University of Science & Technology, Sector 15, Uttara, Dhaka, Bangladesh

[4]Centre for Advanced Research in Sciences (CARS), University of Dhaka, Dhaka 1000, Bangladesh

*zahangir@du.ac.bd

Article

https://doi.org/10.31881/TLR.2024.039

Received 21 February 2024; Accepted 16 April 2024; Published 26 April 2024

ABSTRACT

Environmental toxins from textile effluents, including organic contaminants, heavy metals, and dyes, pose significant health risks such as renal illness, allergies, dermatitis, and cancer when released into the aquatic environment. While various dye removal methods exist, adsorption is highlighted as a potentially effective solution due to its low cost, simplicity, and ease of use. An adsorbent of two-dimensional mesoporous Graphene Oxide (GO) was produced using Hummer's method from cost-effective graphite powder. This was then utilized to eliminate the Doracryl Red MD (DRMD) textile dye from the aqueous system. To characterize the synthesized material, XRD, FTIR, and SEM analyses were performed. Zeta Potential and AFM analysis were used to determine surface charge and roughness, respectively. BET analysis was performed to obtain information regarding the surface area and porosity of the mesoporous GO. The highest adsorption capacity for the adsorption of the dye DRMD was found at 917.62 mg/gm. A variety of factors, including the influence of solution pH, adsorbent dosage, adsorption temperature, concentration of dye solution, and contact time, were thoroughly investigated. Adsorption data best fit the Langmuir model and demonstrated pseudo-second-order reaction kinetics. After repeatedly washing used adsorbents with 2% HCl solution, 88.62% of its initial adsorption capacity was retained after the 4th cycle. Hence, the enhanced adsorption capacity and recyclability of Graphene Oxide (GO) render it a promising candidate for the treatment of wastewater polluted with organic dyes.

KEYWORDS

textile dye DRMD, removal, wastewater, adsorbent, graphene oxide

INTRODUCTION

Graphene oxide (GO) is an amorphous and 2D material which is derived from the oxidation of graphite crystals (sp^2 to sp^3 carbon conversion) and it has hydroxyl (-OH), alkoxy (C-O-C), carbonyl (C-O), carboxylic acid (-COOH), and other oxygen-based functional groups at basal and edge planes [1]. These Oxygenated groups offer several advantages compared to pure graphene and make GO useful in a variety of applications due to its solubility, stability in aqueous solutions, high surface area, and

potential for surface functionalization [2]. GO's ability to dissolve in water makes it possible to form stable aqueous colloids, which are necessary for building bigger structures with cheap raw materials like graphite and high-yield chemical processes [3,4]. Another benefit is the high surface area, which makes it suitable for use as electrode materials in batteries, capacitors, and solar cells [5]. Its honeycomb form enables effective adsorption and trapping of organic molecules such as food allergens, pesticides, antinutrients, and dyes and enables other applications such as desalination, water treatment, and intelligent and active packaging [6]. GO also provides a variety of potential for usage as fillers in nanocomposite materials and bio-composites due to the ease with which their surfaces can be functionalized [3]. A variety of sensors and efficient adsorbents based on graphene oxide and its composites are accessible for the detection and elimination of environmental contaminants [7]. Graphene oxide, a nanomaterial with significant potential for air purification, is capable of eradicating organic pollutants, heavy metal ions, and pesticides from the environment [8].

As human society has expanded, the environment has suffered considerably, leaving human health in peril. One of the most important environmental problems on the planet is water contamination [9] Dyes, due to their widespread application in numerous industries such as textiles, cosmetics, paper, plastics, rubber, leather, pharmaceuticals, and food, have been identified as a primary contributor to all forms of water contamination [10]. As per the Bangladesh Textile Mills Association, Bangladesh holds the position of being the world's second-largest exporter of pre-manufactured garments. A total of 1461 textile-related businesses export textiles worth 28 billion USD per year from Bangladesh [11]. Large amounts of wastewater from the textile industry contain various chromophore groups, such as - N = N-, =C = O C-NH, -CH = N-, and C-S in the dye structure. Inevitably, environmental toxins present in the textile effluent such as organic contaminants, heavy metals, and dyes are released in the natural aquatic environment and end up coexisting with other substances in the aqueous solution. Human health is negatively impacted by contaminated water in a variety of ways, including renal illness, allergies, dermatitis, and cancer [12].

Over the years, many dye removal methods have been suggested, including membrane separation, coagulation/flocculation, reverse osmosis, ion exchange, and even biological procedures. Many of these methods have drawbacks such as high energy usage, challenging design, and lengthy operation times [13]. Among these approaches, adsorption stands out as a potentially helpful one because of its low cost, simplicity, and ease of usage [14]. For the adsorptive removal of organic contaminants from water, carbon-based nanomaterials such as porous carbon, charcoal, bio-char, and activated carbon are frequently utilized [15]. They are desirable because they are inexpensive, have a large surface area, are simple to modify, and have a stronger affinity for environmental pollutants [16]. Despite the high frequency of studies concentrating on the elimination of model dyes used in laboratories, the

exploration of Graphene Oxide-based adsorbents as an option for the removal of commercially prevalent dyes has been relatively under-researched [17].

In the context of this investigation, a two-dimensional mesoporous Graphene Oxide (GO) adsorbent was synthesized to augment the adsorption of a commercially available basic dye, Doracryl Red MD (DRMD), from an aqueous medium. This dye is a commercial textile dye which is widely used in Bangladesh for dying textile fabric. This is a modification of a popular basic dye, Basic Red 46 [18]. GO is characterized by a substantially high surface area as well as exceptional surface roughness attributes. The presence of a multitude of functional groups is the reason behind the high adsorption capacity of GO. Microscopic images proved the layered structure of GO and BET analysis revealed the mesoporous characteristics of the material. Lastly, to comprehend the chemical reactions involved in the dye's removal, thermal parameters, kinetic models and adsorption isotherms were extensively studied.

EXPERIMENTAL

Chemicals

A textile dye, Doracryl Red MD (DRMD) (manufactured by Archroma, Switzerland), was procured from a local dyeing facility in Bangladesh. This dye is categorized under Basic Red 46.

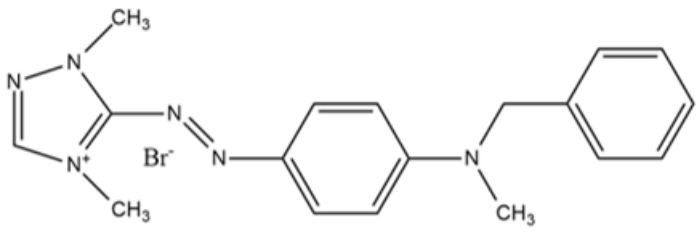

Figure 1. Doracryl Red MD dye chemical structure, Chemical Name: (5-[[4-[Benzylmethylamino]phenyl]azo]-1,4-dimethyl-1H-1,2,4-triazolium trichlorozincate(1-))

Sodium nitrate was purchased from Uni-chem (China). Graphite Powder (with a particle size of ≤50 µm and a purity of 99.5% was sourced from Merck (India). Lastly, chemicals such as Sulfuric Acid (98%), Hydrochloric Acid (37%), Nitric Acid (65%), Potassium Permanganate and Hydrogen Peroxide (30%), were obtained from Merck (Germany).

Preparation of Graphene Oxide

We prepared our GO from inexpensive graphite powders using a modified Hummers method [19,20]. With vigorous shaking in a round-bottomed flask, 3.0 g of graphite powder was added into a 75 mL acid

mixture (concentrated H_2SO_4 and HNO_3 in a 3:1 ratio). Then, 9 gm of $KMnO_4$ and 1.5 gm of $NaNO_3$ were gradually added into the mix. Overnight, it was swirled to produce a thick mix. After that, 150 mL of DI water was added and the mixture was stirred until it was a dark brown colour. 420 mL of DI water was used to dilute it and 80 mL of 30% H_2O_2 was then added and the color swiftly turned into vivid yellow. At last, manganese ions were removed using 200 mL of 5% HCl. GO suspension was neutralized by washing it several times with DI water.

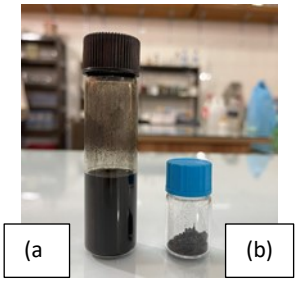

Figure 1. Graphene Oxide dispersed in water (a) and in dried powder form (b)

Characterization of Prepared Mesoporous Adsorbent

FTIR, XRD and AFM were conducted at the University of Dhaka. Zeta potential determination and Raman spectroscopy were done at the Atomic Energy Centre, Dhaka. The sample was imaged using FESEM at Bangladesh University of Engineering Technology. Bangladesh Council of Scientific and Industrial Research (BCSIR), Dhaka assisted in carrying out BET analysis of the sample.

Elemental Analysis

Elemental analyzer (Model: varioMicro V1.6.1GmbH, Germany) revealed the composition of GO. Combustion temperature was set to 1150 °C and a thermal conductivity detector was used.

FTIR Analysis

The chemical structure of GO and the presence of different functional groups were analyzed using IR Prestige-21, SHIMADZU, and Japan Fourier Transformed Infrared (FT-IR) spectrophotometer.

XRD Analysis

X-ray diffraction analysis was carried out using Ultima IV, Rigaku Corporation, Japan X-ray diffraction machine.

Raman Spectroscopy

Raman spectroscopy was used to determine if G-band and D-band were present in GO and carried out using MonoVista CRS+, Spectroscopy & Imaging GmbH, Germany.

FESEM Imaging

The microstructure, morphology and interlayer layer distance of GO were studied with a Field Emission Scanning Electron Microscope (FESEM) (Instrument model: JSM 7600F, JEOL-Japan). Images utilizing Field Emission Scanning Electron Microscopy (FESEM) were obtained at varying magnifications, ranging from 500x to 50,000x. This was done to gain a comprehensive understanding of the structure of the synthesized Graphene Oxide (GO) from multiple perspectives. These produced images helped to study and understand the microstructure and morphology of GO.

AFM Analysis

The prepared GO's surface roughness was measured by Nanosurf Acoustic Enclosure 100, Switzerland Atomic Force Microscope (AFM).

Zeta Potential Analysis

Malvern Zetasizer Nano-ZS analyzer was applied to find the variance in GO's Zeta potential with the measured pH.

BET Surface Area Analysis

Using a BET Sorptometer, the Specific Surface Area, Total Volume, and Average Pore Diameter of the prepared adsorbent surface were measured (Instrument model no: BET-201-A, PMI, USA). In this experiment, nitrogen gas was used as adsorbate.

Cytotoxic Effect Analysis

The cytotoxic effect of the effluent after adsorption was examined using the Vero cell line, a kidney epithelial cell extracted from an African green monkey.

Adsorption Study

The impacts of many parameters, including the dosage of adsorbent, pH, initial dye concentration, temperature, and contact time, were examined to determine the optimal adsorption state for DRMD on GO. The effects of pH values between 2.0 and 10.0 were studied. The initial adsorbent doses were 2.5 to 25 mg in 10 mL of dye solution to study the effects of the dosage. The effect of adsorption time and dye concentration was carried out using 300, 400, 500 and 600 ppm solutions with intervals from 10 to 90 minutes. Thermodynamics of the study were examined at 301 K, 313 K, and 323 K. The adsorbent was separated using filtration. By using a UV-1700 Pharma Spec Spectrophotometer from SIMADZU, Japan, a spectroscopic approach was used to determine the final dye concentration.

Accordingly, a value of 529 nm was determined for adsorption maxima. The adsorption capacity, q (mg/g), was calculated using the following Eq. 1.

$$q = (C_o - C_t) \times \frac{V}{W} \quad (1)$$

$$q_e = (C_o - C_e) \times \frac{V}{W} \quad (2)$$

Where C_o represents the initial concentration of the dye (in ppm), C_t denotes the concentration of the dye (in ppm) at a given time (t), and C_e represents the concentration of dye (ppm) at equilibrium conditions. V is the volume (in L) of the dye solution, and W signifies the mass (in g) of the adsorbent. Equation (2) was used to calculate equilibrium adsorption capacity, q_e (mg/gm)

The dye removal percentage is determined by

$$\% \text{ removal } = \frac{(C_o - C_t)}{C_o} \times 100 \quad (3)$$

For each experiment, a blank was conducted to nullify any error caused by the removal of dye due to any method other than adsorption by GO. The concentrations of GO used in the dye adsorption study were in line with the previous studies [21,22].

Effect of pH on Adsorption

To examine how pH affects the adsorption of the dye DRMD by GO, a total of nine experiments were conducted. In 9 volumetric flasks, 20 mL, 900 ppm dye solutions were used to vary pH from 2.0 - 10.0 with 1 per cent (w/v) HCL and 0.5 per cent NaOH solutions. Adding 20 mg well-dispersed GO to solutions, transferred to 50 mL conical flask and then, shaken at 180 rpm for 30 minutes. The final concentration was determined spectrophotometrically and subsequently, the adsorption capacities at various pH levels were determined utilizing Equation 1.

Effect of Dosage

A total of six tests were carried out to identify the optimal amount of GO for absorption. In 50 mL conical flasks, 10 mL of dye solutions were introduced. The pH was then regulated, followed by the addition of dispersed GO in varying quantities (2.5, 5, 7.5, 10, 15, or 20 mg). These mixtures were then agitated at a rate of 180 rpm for thirty minutes. The exhausted adsorbents were isolated, and the concentrations of the solutions were ascertained via UV-visible spectroscopy. The standard calibration

curve served as the basis for determining these solution concentrations. Adsorption capacities and removal percentages were determined using Equations 1 and 3. The optimal dose was found by identifying the intersection point.

Effect of Contact Time and Initial Dye Concentration

Using 20 mL of 300 ppm dye solutions supplied to 5 conical flasks at pH 7.0, it was possible to examine the effects of dye concentration and contact time on DRMD adsorption onto GO. 10 mg dispersed GO was added to each solution, shaken at 301 K (28 °C) for 5 to 40 minutes at a speed of 180 rpm. After shaking and removing the spent adsorbent, concentrations of final dye solutions were determined using UV-Vis spectroscopy at 529 nm. Equation 1 was used to determine adsorption capabilities at different contact times. 500, 600, and 700 ppm dye solutions were tested similarly.

Thermodynamic Study of Dye Adsorption

This study examined temperature-related effects on dye adsorption at three temperatures (301 K, 313 K and 323 K). In addition, the Gibbs free energy (ΔG), average standard enthalpy change (ΔH), and entropy change (ΔS) were estimated. The adsorption process is assumed based on variations in Gibb's free energy (ΔG). Physical adsorption is indicated by a rise in G values with increasing temperature, and the process is favoured at low temperatures. Changes in Gibb's free energy can be calculated by

$$\Delta G = -RT \ln k_d \tag{4}$$

where the constant (k_d) represents the distribution for equilibrium adsorption. The universal gas constant, denoted as (R), is (8.314 J mol-1 K^{-1}), and (T) signifies the absolute temperature in Kelvin. The calculation of (k_d) was performed using a specific equation.

$$k_d = \frac{q_e}{C_e} \tag{5}$$

By applying the Van't Hoff equation, we were able to ascertain the mean standard changes in enthalpy (ΔH) and entropy (ΔS) associated with the adsorption process.

$$\ln k_d = \frac{-\Delta H}{RT} + \frac{\Delta S}{R} \tag{6}$$

Plotting lnk_d versus 1/T resulted in a straight line. The slope and intercept were used to calculate the value of standard enthalpy change ΔH and entropy change ΔS, respectively.

Studying Adsorption Isotherm

Obtained data were tested onto both Langmuir and Freundlich adsorption isotherms. The linear form of the Langmuir isotherm is

$$\frac{C_e}{q_e} = \frac{1}{q_m b} + \frac{1}{q_m} C_e \quad (7)$$

where, b = Langmuir constant, C_e = equilibrium concentration, q_m = the maximum theoretical adsorption capacity and q_e = equilibrium adsorption capacity. R_L, the separation factor, can be linked to b through the following formula where C_m is the maximum dye concentration

$$R_L = \frac{1}{1 + C_m b} \quad (8)$$

The following equation can represent the Freundlich adsorption isotherm.

$$ln\, q_e = ln\, k_F + \frac{1}{n} ln C_e \quad (9)$$

Studying Adsorption Kinetics

This study used two kinetic models to explain adsorption. Ho, Mckay, and Lagergren introduced pseudo-second and pseudo-first order rate equations respectively, to characterize the kinetic process. Pseudo-first-order rate equation in its linear form

$$log(q_e - q_t) = log\, q_e - \frac{k_1}{2.303} t \quad (10)$$

where, q_t = adsorption capacity at time t, q_e= equilibrium adsorption capacity and, k_1= rate constant of pseudo-first order adsorption (L/min).

Pseudo-second-order rate equation in the linear form:

$$\frac{t}{q_t} = \frac{1}{k_2 q_e^2} + \frac{1}{q_e} t \quad (11)$$

where k_2 = pseudo-second-order rate constant for adsorption (g/mg min).

Regeneration

The employed Graphene Oxide (GO) underwent a treatment with 2% HCl for dye removal during the regeneration phase. Subsequently, the pH was fine-tuned using distilled water until it achieved a value of 7.0. The regenerated GO, after being dried, was repurposed for further adsorption. In this particular study, a dispersion of 10 mg of the regenerated GO was used for a 20 mL solution of dye with a concentration of 300 ppm at a pH of 7.0, and this mixture was subjected to shaking for 30 minutes.

RESULTS AND DISCUSSION

Characterization

The elemental analysis result showed that the GO sample contained 54.94% C, 1.947% H, 4.22% N and 0.766% S. Furthermore, this suggests that a large proportion of Oxygen is present (38.127%).

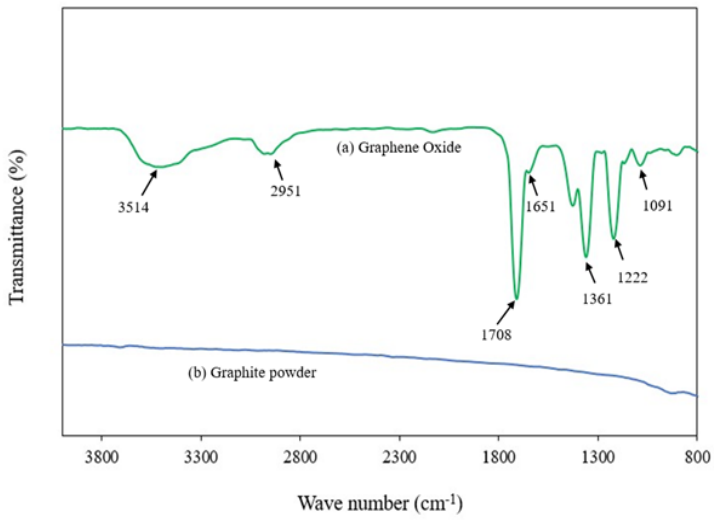

Figure 2. FTIR spectra of Graphene Oxide (denoted as (a)) and Graphite powder (referred to as (b))

In the case of Graphene Oxide (GO), the positions of the vibrational peaks were identified at the following wavenumbers: 1091 cm^{-1}, 1222 cm^{-1}, 1361 cm^{-1}, 1427 cm^{-1}, 1651 cm^{-1}, 1708 cm^{-1}, 2951 cm^{-1}, 3514 cm^{-1} (Fig. 3(a)). These peaks are attributed to Carboxy C-O stretching, C-O stretching (alkyl aryl ether), C-O-H bending (alcohol), C-O-H bending (carboxylic acid), Aromatic C=C stretching, Carbonyl C=O stretching, C-H stretching and -OH groups, respectively. The collected data revealed the

presence of both -COOH and -OH groups in GO. However, these functional groups were not present in the starting material, Graphite powder, as shown in Fig. 3 (b). This suggested that under the reaction protocol, oxidation of graphite powder took place and it was converted to GO. These experimental values were in close agreement with the peak values of the FTIR spectra matching the earlier studies [23,24].

The FESEM images (Fig. 4) showed that the GO had a fluffy and layered structure, with numerous wrinkled laminae. These sheets suggested a large surface area and layered morphology, which would result in a greater adsorption capacity for the material. The fluffiness and wrinkles in the GO were believed to have been caused by oxidation and layer separation. Images of the layer structures of GO have been obtained in many working experiments, and these observations correlated well with our experimental findings [25]. Using ImageJ software, the thickness of the GO sheets was measured from these images. The mean thickness was calculated to be 691.042 nm by analyzing several cross-sectional view shots.

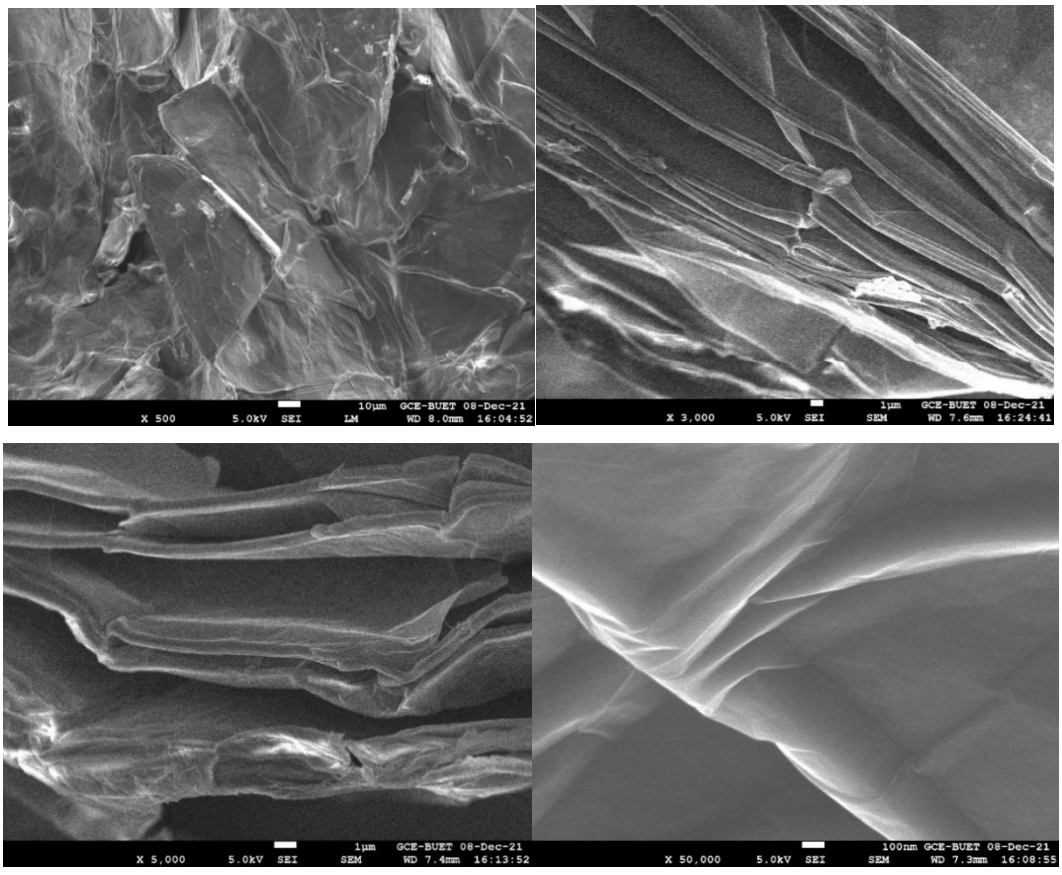

Figure 3. Field Emission Scanning Electron Microscopy (FESEM) imagery of Graphene Oxide

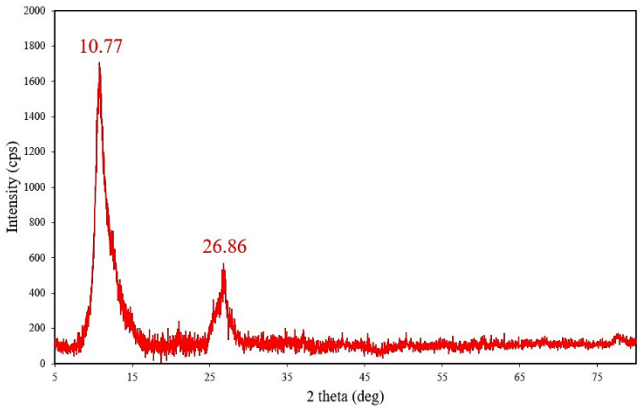

Figure 4. X-ray Diffraction (XRD) patterns associated with Graphene Oxide

The XRD analysis of GO was performed to examine the distance between the layers of GO sheets. The results shown in Fig. 5 revealed a broad peak at 2Θ = 10.77° corresponding to an interlayer spacing of 8.25 Å. This spacing was significantly larger than that of graphite reported in previous studies [26]. This is thought to be a result of the disintegration of graphite's crystalline structure and the emergence of more amorphous formations in GO. A minor peak at 2Θ = 26.76° is due to some unreacted graphite powders.

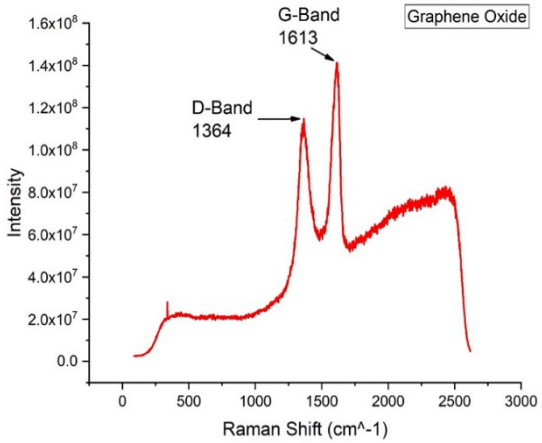

Figure 5. Raman Spectrum on Graphene Oxide

As depicted in the Raman spectrum (see Fig. 6), the G-band and D-band were situated at 1613 cm^{-1} and 1364 cm^{-1}, respectively. In the case of Graphene Oxide (GO), the intensity proportion of the D-band to the G-band (I_D/I_G) was noted to be 0.81. The G-band and D-band peak values, as well as the I_D/I_G value, are in close alignment with earlier research [27,28]. The emergence of the D-band authenticated the existence of imperfection sites within the GO laminae, as well as the dimensions of the in-plane sp^2 domain [29].

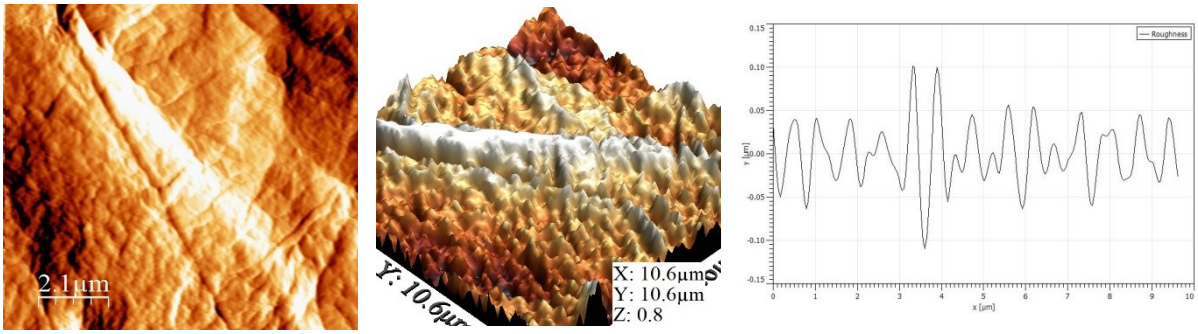

(a) (b) (c)

Figure 6. Two-dimensional (2D) (represented as (a)) and three-dimensional (3D) (denoted as (b)) topographic images, along with the Roughness profile (indicated as (c)) of GO, as derived from Atomic Force Microscopy (AFM)

The topographic image derived from AFM (Fig. 7) was used to conduct a quantitative analysis of the surface roughness at the nanoscale and to depict the nano-texture of the surface. The images revealed a stratified structure with a rough texture for the synthesized GO, which aligned with the observations from the SEM images. The average roughness (R_a) was determined to be 85.92 nm, while the mean surface roughness (S_a) was found to be 238.2 nm. The surface roughness and structure of GO were consistent with earlier research [30,31]. The surface had become highly rough due to the intense oxidation process using strong acids as evidenced by the R_a and S_a values. This highly rough surface was ideal for the adsorption of various pollutant molecules.

Table 1. Different surface area and porosity properties obtained from BET analysis data of GO

Test Parameter	BET Specific Surface Area using multi-point analysis (m^2/g)	Total Pore Volume (cc/g)	Skeletal density (g/cc)	Porosity based on skeletal density (per gram of sample)	Average Pore Diameter, 4V/S (nm)
Sample: GO	95.85	0.1004	0.5	0.0478	4.189

The BET data presented in Table 1 revealed that the average pore diameter was 4.189 nm, a feature indicative of mesoporous material. Mesoporous material pore diameters typically range from 2 nm to 50 nm. Mesoporous materials have large accessible surface areas and variable pore diameters, which are particularly favourable for mass transport and electron/reactant dispersion [32]. Therefore, the prepared GO adsorbent exhibited a high accessible surface area, which is a desirable property of adsorbent.

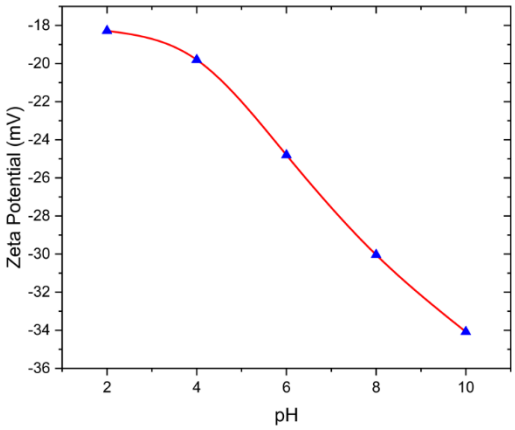

Figure 7. Zeta potential values corresponding to GO at varying pH levels

During the Zeta Potential analysis, the pH was adjusted from 2.0 to 10.0. The results, presented in Fig. 8, showed that the zeta potential values of GO were consistently negative across all pH levels, ranging from -18.28 to -34 mV as the pH increased from 2.0 to 10.0. The zeta potential values at different pH were in good agreement with the previous results described in relevant research [33–35].

No cytotoxic effect was observed for the GO sample solution with >95% survival of Vero cells.

Adsorption of Doracryl Red MD on Mesoporous Graphene Oxide

Effect of pH on Adsorption Capacity

The maximum adsorption capacity of GO was found to be 898.99 mg/gm at pH 10.0 (Fig. 9). As pH increased from 2.0 to 10.0, the adsorption capacity also increased, with a relatively stable capacity between pH 4.0 to 7.0, where it varied by only 23.02 mg/gm. At pH 7.0, which is easy to achieve and maintain, GO showed a high adsorption capacity of 813.21 mg/gm, only 85.78 mg/gm less than the maximum capacity. Since it is easy to achieve and maintain a neutral pH, the rest of the study was conducted at pH 7.0.

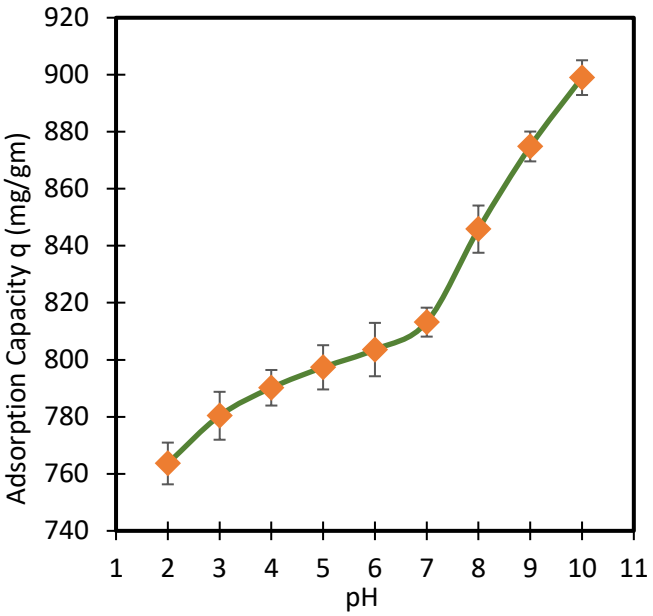

Fig. 8 Impact of pH fluctuations on the adsorption capacity

pH level plays a crucial role in adsorption studies as it can significantly alter the surface charge of the adsorbent and adsorbate. At elevated pH levels, GO's carboxyl groups extensively disintegrate, leading to a highly negatively charged surface. This facilitates the interaction between the negatively charged surface and the cationic dye (Dye+). However, at lower pH levels, some of GO's carboxyl groups become protonated, forming positive ions (Fig. 10). This results in an electrostatic repulsion between the cationic dye and the adsorbent, thereby reducing adsorption [36].

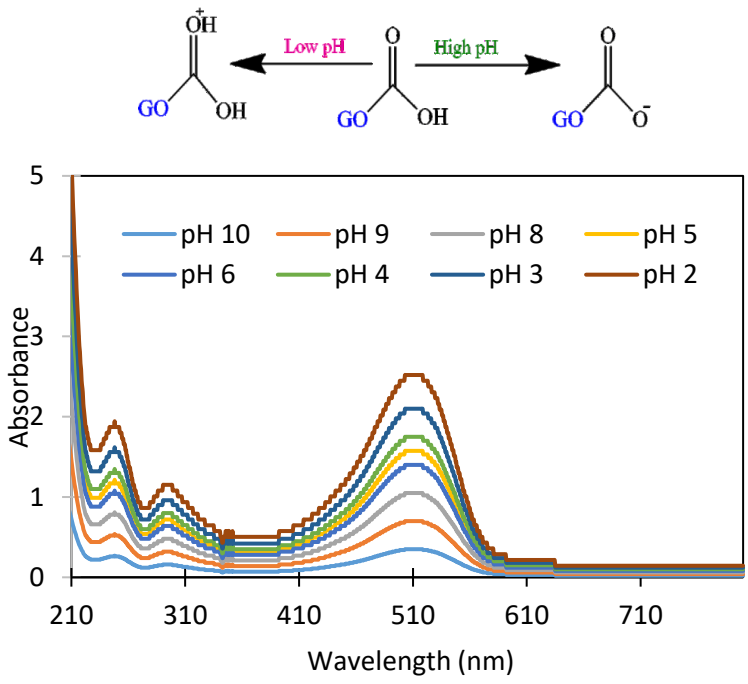

Figure 9. Effect of varying pH on the surface charge of GO adsorbent

Effect of Varying Adsorbent Dosage on Adsorption Capacity and Percentage Dye Removal

The empirical findings (refer to Fig. 11) indicated an inverse relationship between the dosage of the adsorbent and its adsorption capacity. At lower dosages, the concentration gradient between the adsorbent surface and the bulk solution is quite high, so more dye molecules diffuse towards the adsorbent surface and get adsorbed. In this scenario, the small quantity of adsorbent can use its full potential. Conversely, the proportion of dye removal escalated with an increase in the adsorbent dosage. A higher amount of adsorbent meant more dye was removed from the solution, making the final concentration low. A solution dosed at 6.4 mg/10 mL demonstrated superior adsorption capacity and the most effective dye removal percentage.

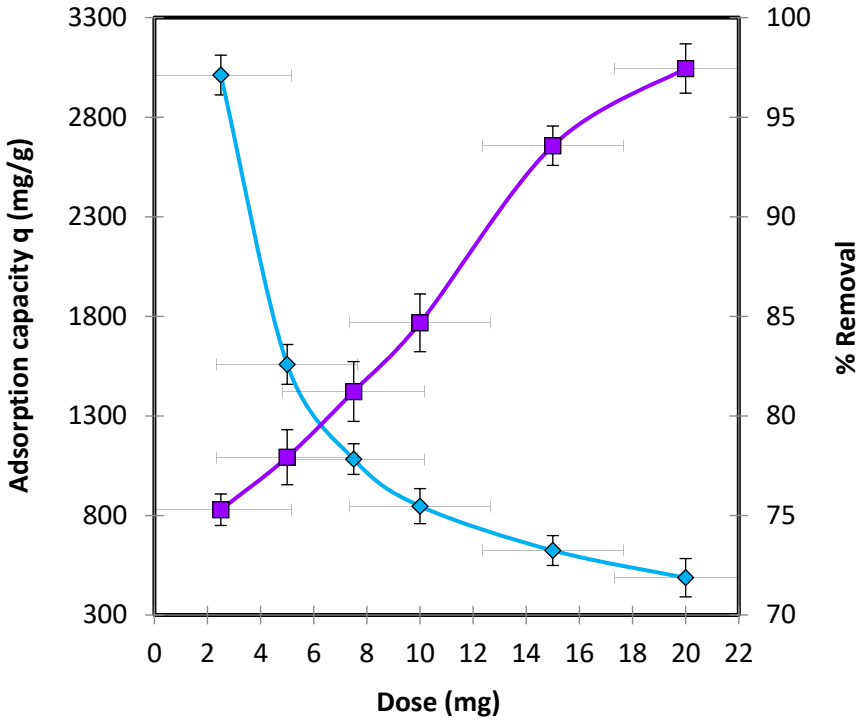

Figure 1. Effect of different dosages on adsorption capacity and % removal

Effect of Contact Time and Initial Dye Concentration

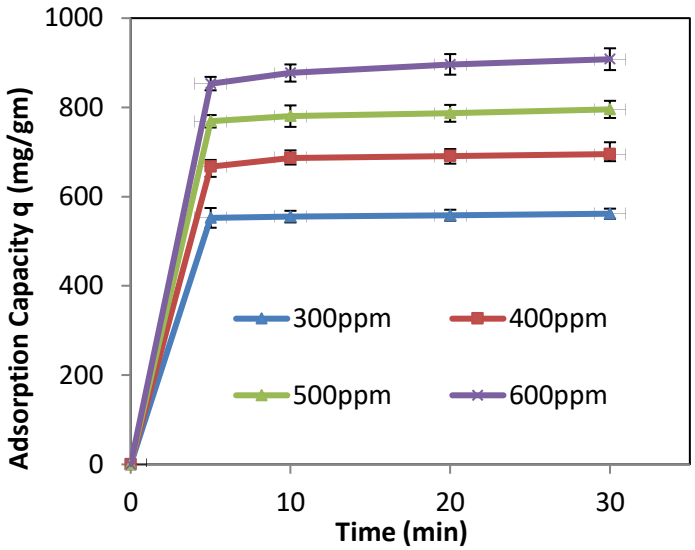

Figure 11. Effect of initial solution concentration and adsorbent-adsorbate contact time on adsorption

During these experiments, there was a noted increase in adsorption capacity over time, attributable to the presence of a greater number of active sites (as depicted in Fig. 12). However, with the progression of time, these sites reached a state of saturation, culminating in an adsorption capacity that remained nearly constant. Furthermore, an escalation in the initial dye concentration corresponded to an increase in the adsorption capacity. This can be explained by the heightened concentration gradient between the dye molecule in the bulk solution and the surface of the adsorbent, which facilitated a more substantial mass transfer between the liquid and solid phases [37].

Thermodynamic Analysis

The equilibrium adsorption capacity was found to be 813.88 mg/gm at 301 K decreased to 758.89 mg/gm and 654.39 mg/gm at 313 K and 323 K respectively (Fig. 13). At 301K, 313K, and 323K, Gibb's free energies were determined to be, respectively, -5.42, -4.785, and -3.575 KJ/mol.

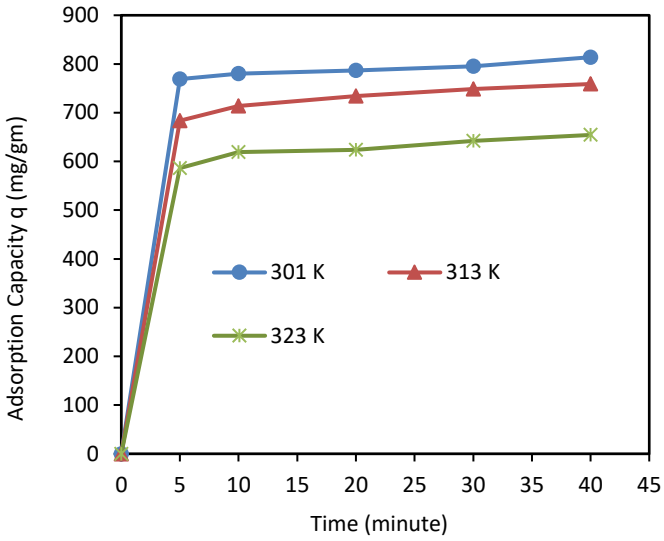

Figure 12. Effect of temperature on adsorption

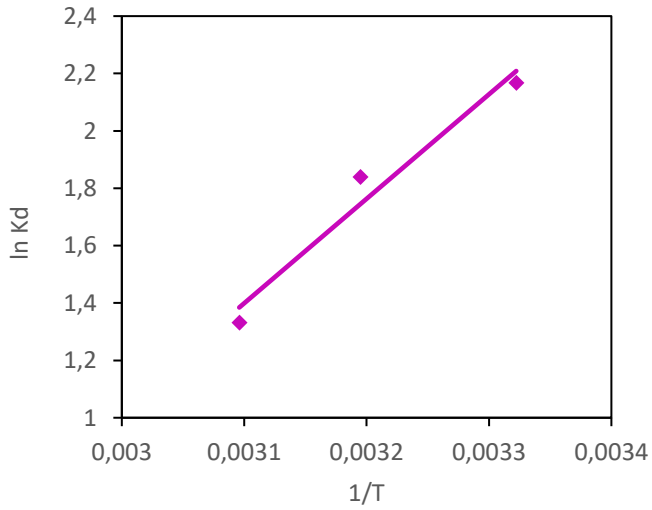

Figure 13. Graphical representation of the Van't Hoff equation for the adsorption process

According to the van't Hoff equation plot (Fig. 14), the standard enthalpy change (ΔH^o) was determined to be -30.28 KJ/mol and the entropy change (ΔS^o) was -0.082 KJ/Kmol. As the temperature increased from 301 K to 323 K, the value of ΔG^o changed from -5.42 KJ/mol to -3.58 KJ/mol, indicating that the adsorption was spontaneous at lower temperatures and its nature was physical [38].

Adsorption Isotherms

Langmuir's isotherm is based on the idea that adsorbate molecules stick to well-defined, energetically equal sites in a single layer, with no interaction between the molecules [39]. The Langmuir model was evaluated using Equation 7, which involved plotting C_e/q_e against Ce. A linear correlation was discerned between C_e/q_e and C_e (as illustrated in Fig. 15), with a satisfactory regression coefficient ($R^2 = 0.9981$).

The slope of this plot yielded the theoretical maximum adsorption capacity, denoted as q_m, which was determined to be 1000 mg/gm.

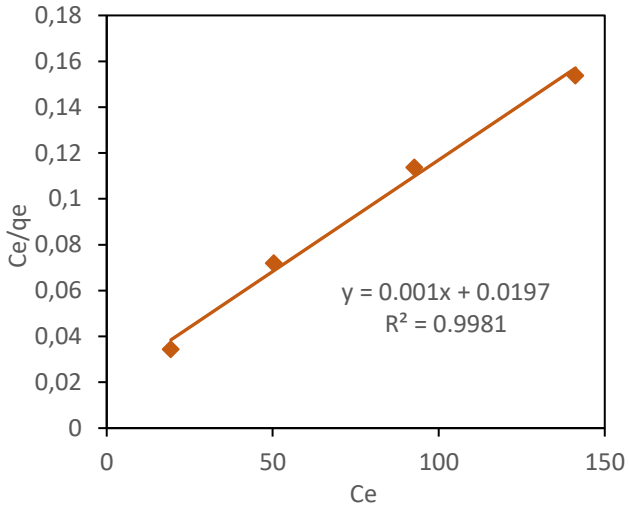

Figure 14. Langmuir adsorption isotherm for adsorption of the dye at 301 K

The separation factor, denoted as (R_L), is associated with the Langmuir constant and serves as a qualitative indicator of the favorability of the adsorption process. An (R_L) value exceeding 1 signifies unfavourable adsorption, whereas an (R_L) value between 0 and 1 suggests a favourable process. The (R_L) value was computed using Equation 8. With an (R_L) value of 0.03179, the process indicates highly favourable monolayer adsorption [40].

Freundlich isotherms assume multilayer adsorption with uneven distribution of adsorbents [41]. By plotting $\ln C_e$ vs $\ln q_e$, the experimental results were further examined for the multilayer adsorption process using the Freundlich isotherm with Equation 9. A linear association with a decent regression coefficient (R^2 = 0.9934) was obtained (Fig. 16). Using Equation 9, the value of n was computed and found to be 4.0733, suggesting that the adsorption was moderate to good. Adsorption gets more challenging as n declines (excellent adsorption at n = 2 - 10, difficult adsorption at n = 1 - 2, and poor adsorption at n<1) [40].

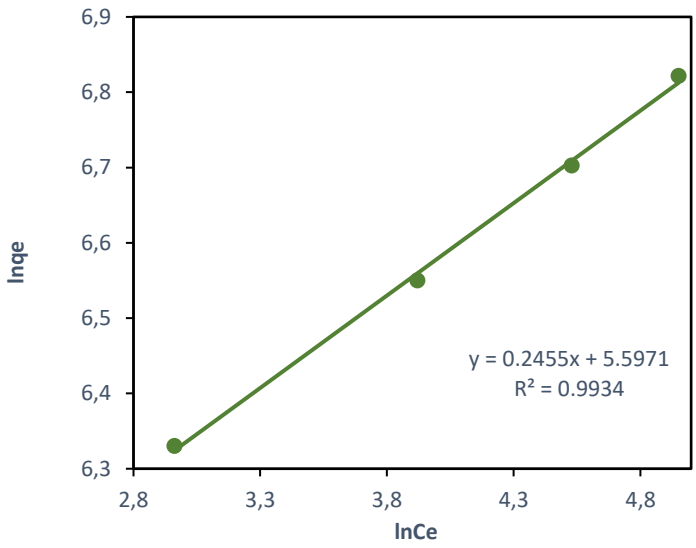

Figure 15. Freundlich adsorption isotherm for adsorption of the dye at 301 K

Table 2 encompasses the values for various parameters on both the Langmuir and Freundlich isotherms. Based on the information presented in the table, it can be inferred that the adsorption process adheres to both the Langmuir and Freundlich models.

Table 2. Theoretical values obtained from Langmuir and Freundlich isotherm for adsorption of dye DRMD on GO at 301 K

	q (mg/gm)	R^2	b Lmg^{-1}	R_L	n	K_F
Langmuir Isotherm	1000	0.9981	0.5076	0.03179	-	-
Freundlich Isotherm	-	0.9934	-	-	4.0733	269.64

Adsorption Kinetics for Adsorption

The pseudo-first-order model was obtained by plotting $\log(q_e-q_t)$ versus t according to Equation 10 where a linear relationship between $\log(q_e-q_t)$ and t was observed (Fig. 17).

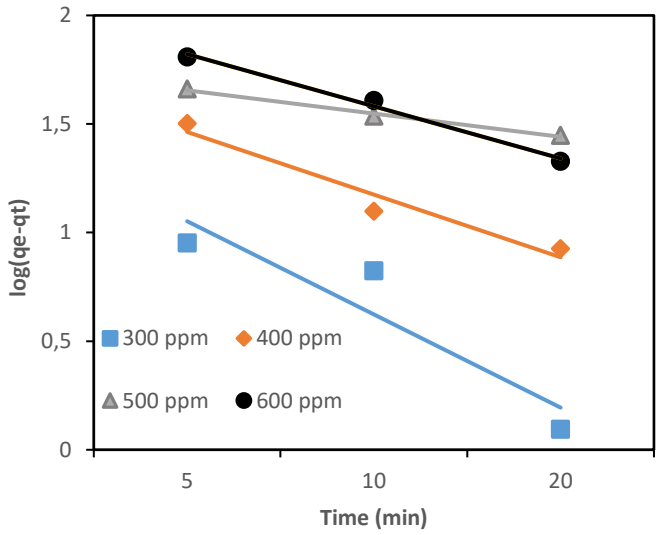

Figure 16. Pseudo-first order adsorption kinetics for adsorption of the dye at 301 K

Pseudo-second-order model was obtained by plotting t/q_t versus t according to Equation 11. The plot was a combination of straight lines for all four concentrations (Fig. 18).

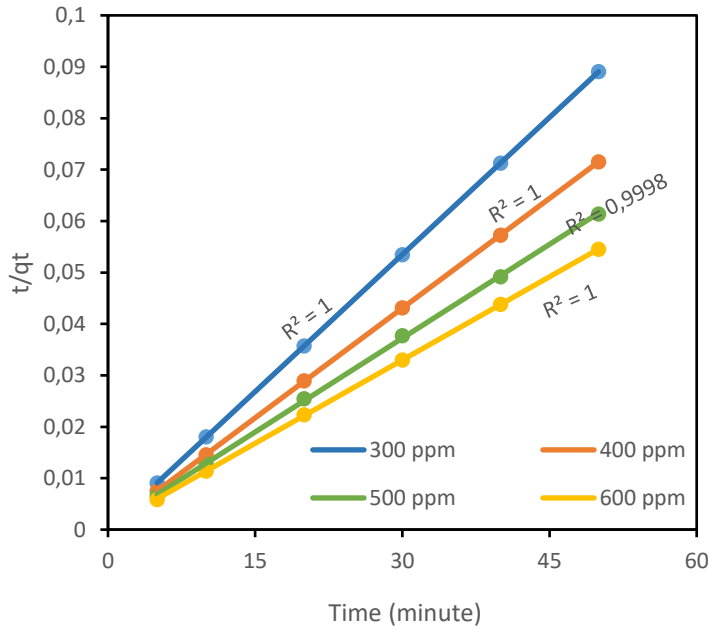

Figure 17. Pseudo-second order adsorption kinetics for adsorption of the dye at 301 K

Table 3. Parameters of kinetics for both Pseudo-first-order and Pseudo-second-order reactions during the adsorption process of the dye DRMD on GO

Name of Kinetic Model	Parameters	Initial Concentration of Dye			
		300 ppm	400 ppm	500 ppm	600 ppm
Pseudo-first order	q_e, exp (mg/gm)	561.35	699.25	814.71	917.62
	q_e, cal (First-order)	30.29	56.44	57.82	115.34
	K_1	0.988	0.664	0.246	0.553
	R^2	0.859	0.949	0.990	0.991
Pseudo-second order	q_e, cal (Second-order)	555.56	714.29	833.33	909.09
	K_2	0.016	0.005	0.002	0.002
	R^2	1	1	0.9998	1

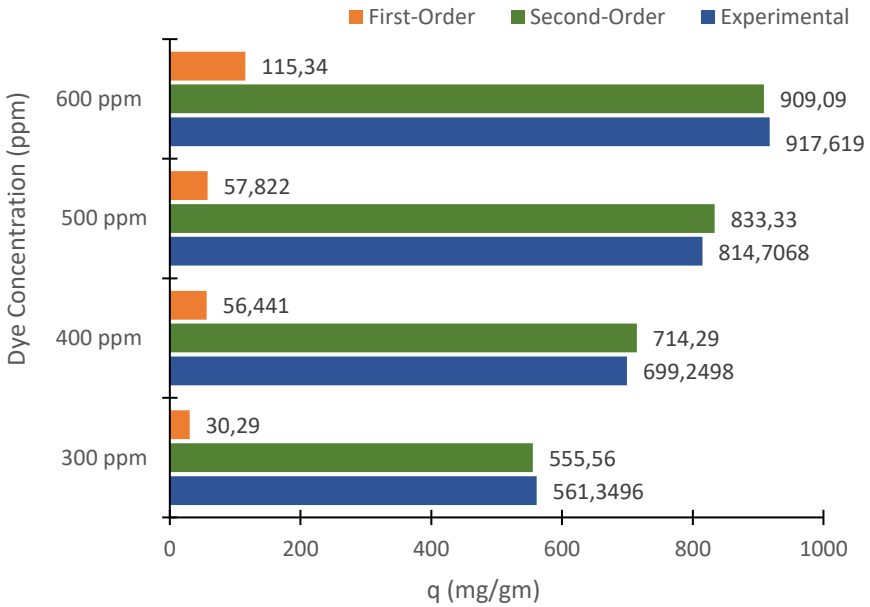

Figure 18. A comparative analysis of the adsorption capacities for dye DRMD on Graphene Oxide (GO) under pseudo-first-order and pseudo-second-order kinetic

The kinetic parameters for the adsorption process are outlined in Table 3. Both Table 3 and Fig. 19 indicate that the calculated adsorption capacity aligns well with the actual values for pseudo-second-order kinetics. This alignment leads to the inference that the adsorption process in this study adheres to pseudo-second-order kinetics.

Regeneration of the Adsorbent

The initial Graphene Oxide (GO) demonstrated an adsorption capacity of 596.6116 mg/gm for a dye solution with a concentration of 300 ppm. However, the regenerated GO, after the 1st, 2nd, 3rd, and 4th cycles, exhibited adsorption capacities of 561.3858 mg/gm, 545.0324 mg/gm, 533.7284 mg/gm, and 528.715 mg/gm respectively (refer to Fig. 20). So, after using the adsorbent for the 4th time, the

adsorbent retained 88.62% of its initial adsorption capacity which is a clear indication towards the reusability of GO for the removal of industrial dye DRMD.

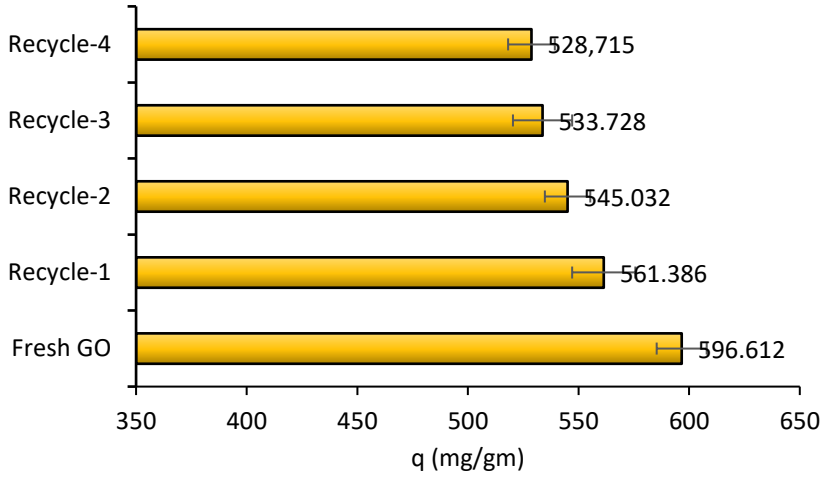

Figure 19. Recyclability potential analysis of GO

Plausible Mechanism for the Adsorption Process

After evaluating all the characterization results, it can be realized that the adsorbent used here, GO, had a very rough surface and high surface area with lots of oxygen-containing groups. The adsorbent material was mesoporous and had a high specific surface area and total pore volume. In the aqueous medium, the surface -COOH and -OH groups got dissociated and imparted a negative surface charge. On the other hand, the industrial dye DRMD existed as a cation in the solution. So, due to the electrostatic force of attraction, dye molecules got adsorbed on the surface of the adsorbent. As the pH of the solution was increased, more and more carboxyl groups were dissociated, making the surface more negatively charged. So, adsorption capacity increased with increasing pH. This mechanism is demonstrated in Fig. 21.

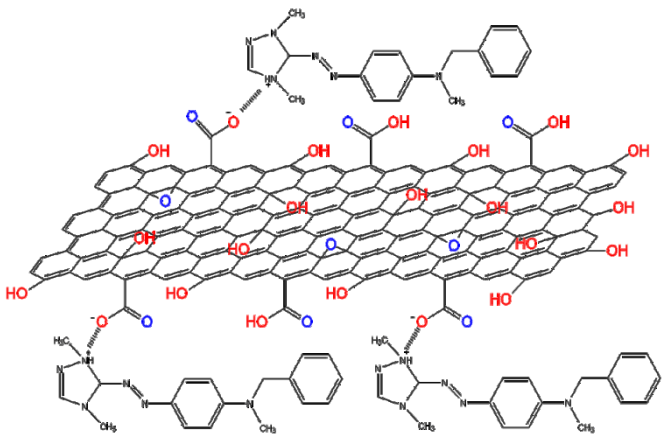

Figure 20. The mechanism showing the absorption process of DRMD dye by the Graphene Oxide (GO) adsorbent

The following chart represents a comparison between different recently developed adsorbents with GO prepared in this research.

Table 4. Cationic dye adsorption capacity of different recently developed adsorbents

Name of adsorbent	Adsorption capacity (mg/gm)	Reference
Rubber seeds	Methylene Blue: 769.23	[42]
Activated Carbon from fuel oil	Rhodium 6G: 27-18	[43]
Amberlite ®IRC-50	Safranin (SF): 39	[44]
Activated carbon (MTLAC) and sulfonic acid-modified activated carbon (MTLAC-SA)	Rhodamine B (RhB): 757.6	[45]
Peroxide-treated rice husk	Malachite green (MG): 26.6	[46]
CsTC2 [chitosan (Cs), talc (T), and Cloisite 30B clay (C)]	Crystal violet (CV): 37.03	[47]
Magnetic Calcium Alginate-Graphene Oxide Composite	Doracryl Red MD (DRMD): 1428.57	[20]
Graphene Oxide (GO)	Doracryl Red MD (DRMD): 917.62	Current Research

The table indicated that the adsorption capacity for the prepared GO is the second highest among other adsorbents in the chart. The dye used here for the experiment was a commercial textile dye applied for dying in factories in Bangladesh and was more practical to use in the case of this study.

CONCLUSION

Graphene Oxide is useful in a variety of applications due to its solubility, stability in aqueous solutions, high surface area, and potential for surface functionalization. Many efficient adsorbents based on graphene oxide are accessible for the elimination of environmental contaminants, such as textile dyes. Two-dimensional mesoporous GO was synthesized in this study and it was employed to adsorb textile dye DRMD from aqueous medium. As DRMD is used in dying industries in Bangladesh for dying fabric, the results obtained here can be useful in minimizing water pollution. The adsorption procedure adhered to the kinetics of a Pseudo-second order reaction, and the adsorption data was in line with both the Langmuir and Freundlich adsorption isotherms. As the pH escalated, there was a corresponding increase in the adsorbent's adsorption capacity. This adsorption process was revealed to be spontaneous and exothermic based on the thermodynamic analysis, with very high initial adsorption of the dye molecules. In the regeneration test, 88.62% adsorption capacity of the mesoporous adsorbent remained after the 4^{th} cycle. Therefore, mesoporous GO can be employed as a robust adsorbent to remove textile dyes from wastewater. It can treat heavy metals, antibiotics, pesticides, and many other charged organic pollutants because of its wide range of functional groups.

Author Contributions

A substantial part of the literature review was undertaken by Malitha SB, who also executed all the laboratory experiments and wrote most parts of the manuscript. Ria MR was responsible for the literature review and composition of several sections. Mahmudunnabi DM performed a literature review for selected sections. Hossain KS carried out the AFM experiments and undertook the data analysis. Mia MAS reviewed the manuscript and assisted in data analysis. Alam MZ supervised the research work and contributed to the completion of the manuscript. The final manuscript received the approval of all authors after a thorough reading.

Conflicts of Interest

The authors declare that there is no conflict of interest or competing interests.

Funding

This research was funded by the DU 100 years project, University of Dhaka.

Hazards

All the chemicals, procedures or equipment that have been used in this research do not have any unusual hazards inherent in their use.

Availability of data

Data will be made available on request.

Acknowledgements

Bangladesh Council of Scientific and Industrial Research (BCSIR), Atomic Energy Centre, Dhaka, Centre for Advanced Research in Sciences (CARS), University of Dhaka, and Semiconductor Technology Research Centre, University of Dhaka supported this research work.

REFERENCES

[1] Donato KZ, Tan HL, Marangoni VS, Martins MVS, Ng PR, Costa MCF, Jain P, Lee SJ, Koon GKW, Donato RK, Neto AHC. Graphene oxide classification and standardization. Scientific Reports. 2023; 13:1–9. https://doi.org/10.1038/s41598-023-33350-5

[2] Joshi S, Bobade H, Sharma R, Sharma S. Graphene derivatives: Properties and potential food applications. Journal of Industrial and Engineering Chemistry. 2023; 123:1–18. https://doi.org/10.1016/j.jiec.2023.03.047

[3] Smith AT, LaChance AM, Zeng S, Liu B, Sun L. Synthesis, properties, and applications of graphene oxide/reduced graphene oxide and their nanocomposites. Nano Materials Science. 2019; 1:31–47. https://doi.org/10.1016/j.nanoms.2019.02.004

[4] Chen D, Feng H, Li J. Graphene oxide: Preparation, functionalization, and electrochemical applications. Chemical Reviews. 2012; 112:6027–53. https://doi.org/10.1021/cr300115g

[5] Zare P, Aleemardani M, Seifalian A, Bagher Z, Seifalian AM. Graphene oxide: Opportunities and challenges in biomedicine. Nanomaterials. 2021; 11. https://doi.org/10.3390/nano11051083

[6] Farjadian F, Abbaspour S, Sadatlu MAA, Mirkiani S, Ghasemi A, Hoseini-Ghahfarokhi M, Mozaffari N, Karimi M, Hamblin MR. Recent Developments in Graphene and Graphene Oxide: Properties, Synthesis, and Modifications: A Review. ChemistrySelect. 2020; 5:10200–10219. https://doi.org/10.1002/slct.202002501

[7] Albert EL, Che Abdullah CA, Shiroshaki Y. Synthesis and characterization of graphene oxide functionalized with magnetic nanoparticle via simple emulsion method. Results in Physics. 2018; 11:944–950. https://doi.org/10.1016/J.RINP.2018.10.054

[8] Velusamy S, Roy A, Sundaram S, Kumar Mallick T. A Review on Heavy Metal Ions and Containing Dyes Removal Through Graphene Oxide-Based Adsorption Strategies for Textile Wastewater Treatment. The Chemical Record. 2021; 21:1570–1610. https://doi.org/10.1002/TCR.202000153

[9] Bashir I, Lone FA, Bhat RA, Mir SA, Dar ZA, Dar SA. Concerns and threats of contamination on aquatic ecosystems. Bioremediation and Biotechnology: Sustainable Approaches to Pollution Degradation. 2020; 1–26. https://doi.org/10.1007/978-3-030-35691-0_1/TABLES/4

[10] Sakamoto M, Ahmed T, Begum S, Huq H. Water pollution and the textile industry in Bangladesh: Flawed corporate practices or restrictive opportunities? Sustainability. 2019; 11. https://doi.org/10.3390/su11071951

[11] Hossain L, Sarker SK, Khan MS. Evaluation of present and future wastewater impacts of textile dyeing industries in Bangladesh. Environmental Development. 2018; 26:23–33. https://doi.org/10.1016/j.envdev.2018.03.005

[12] Khan F, Khan MS, Kamal S, Arshad M, Ahmad SI, Nami SAA. Recent advances in graphene oxide and reduced graphene oxide based nanocomposites for the photodegradation of dyes. Journal of Materials Chemistry C. 2020; 8:15940–15955. https://doi.org/10.1039/d0tc03684f

[13] Nayeri D, Mousavi SA. Dye removal from water and wastewater by nanosized metal oxides - modified activated carbon: a review on recent researches. Journal of Environmental Health Science and Engineering. 2020; 18:1671–16789. https://doi.org/10.1007/S40201-020-00566-W

[14] Mao B, Sidhureddy B, Thiruppathi AR, Wood PC, Chen A. Efficient dye removal and separation based on graphene oxide nanomaterials. New Journal of Chemistry. 2020; 44:4519–4528. https://doi.org/10.1039/c9nj05895h

[15] Duman O, Diker CÖ, Tunç S. Development of highly hydrophobic and superoleophilic fluoro organothiol-coated carbonized melamine sponge/rGO composite absorbent material for the efficient and selective absorption of oily substances from aqueous environments. Journal of Environmental Chemical Engineering. 2021; 9:105093. https://doi.org/10.1016/J.JECE.2021.105093

[16] Baig N, Ihsanullah, Sajid M, Saleh TA. Graphene-based adsorbents for the removal of toxic organic pollutants: A review. Journal of Environmental Management. 2019; 244:370–382. https://doi.org/10.1016/j.jenvman.2019.05.047

[17] Hassan MM, Carr CM. A critical review on recent advancements of the removal of reactive dyes from dyehouse effluent by ion-exchange adsorbents. Chemosphere. 2018; 209:201–219. https://doi.org/10.1016/J.CHEMOSPHERE.2018.06.043

[18] Basic red 46. C18H21BrN6. CID 12011963. PubChem. Available from: https://pubchem.ncbi.nlm.nih.gov/compound/Basic-red-46

[19] Mahmudunnabi DM, Alam MZ, Nurnabi M. Removal of TURQUOISE GN from aqueous solution using graphene oxide. Desalination and Water Treatment. 2020; 174:389–399. https://doi.org/10.5004/dwt.2020.24867

[20] Malitha SB, Mahmudunnabi DM, Nurnabi M, Alam MZ. Facile Synthesis and Characterization of Magnetic Calcium Alginate-Graphene Oxide Composite for Removal of a Commercial Textile Dye Doracryl Red MD. Water, Air, and Soil Pollution. 2023; 234:1–17. https://doi.org/10.1007/S11270-023-06264-1/METRICS

[21] Zhang W, Zhou C, Zhou W, Lei A, Zhang Q, Wan Q, Zou B. Fast and considerable adsorption of methylene blue dye onto graphene oxide. Bulletin of Environmental Contamination and Toxicology. 2011; 87:86–90. https://doi.org/10.1007/S00128-011-0304-1/FIGURES/6

[22] Bradder P, Ling SK, Wang S, Liu S. Dye Adsorption on Layered Graphite Oxide. Journal of Chemical and Engineering Data. 2010; 56:138–41. https://doi.org/10.1021/JE101049G

[23] Wazir A, Kundi I, Hussain Wazir A, Waseem Kundi I. Synthesis of graphene nano sheets by the rapid reduction of electrochemically exfoliated graphene oxide induced by microwaves. Journal of The Chemical Society of Pakistan. 2016; 38(1):11-16.

[24] Rattana T, Chaiyakun S, Witit-Anun N, Nuntawong N, Chindaudom P, Oaew S, Kedkeaw C, Limsuwan P. Preparation and characterization of graphene oxide nanosheets. Procedia Engineering. 2012; 32:759-764. https://doi.org/10.1016/j.proeng.2012.02.009

[25] Aliyev E, Filiz V, Khan MM, Lee YJ, Abetz C, Abetz V. Structural characterization of graphene oxide: Surface functional groups and fractionated oxidative debris. Nanomaterials. 2019; 9. https://doi.org/10.3390/nano9081180

[26] Ghorbani M, Abdizadeh H, Golobostanfard MR. Reduction of Graphene Oxide via Modified

Hydrothermal Method. Procedia Materials Science. 2015; 11:326–330. https://doi.org/10.1016/J.MSPRO.2015.11.104

[27] Mutalib TNABTA, Tan SJ, Foo KL, Liew YM, Heah CY, Abdullah MMAB. Properties of polyaniline/graphene oxide (PANI/GO) composites: effect of GO loading. Polymer Bulletin. 2021; 78:4835–47. https://doi.org/10.1007/s00289-020-03334-w

[28] Yasin G, Arif M, Shakeel M, Dun Y, Zuo Y, Khan WQ, Tang Y, Khan A, Nadeem M. Exploring the Nickel–Graphene Nanocomposite Coatings for Superior Corrosion Resistance: Manipulating the Effect of Deposition Current Density on its Morphology, Mechanical Properties, and Erosion-Corrosion Performance. Advanced Engineering Materials. 2018; 20. https://doi.org/10.1002/adem.201701166

[29] Chen W, Yan L, Bangal PR. Chemical reduction of graphene oxide to graphene by sulfur-containing compounds. Journal of Physical Chemistry C. 2010; 114:19885–19890. https://doi.org/10.1021/jp107131v

[30] Thema FT, Moloto MJ, Dikio ED, Nyangiwe NN, Kotsedi L, Maaza M, Khenfouch M. Synthesis and characterization of graphene thin films by chemical reduction of exfoliated and intercalated graphite oxide. Journal of Chemistry. 2013. https://doi.org/10.1155/2013/150536

[31] Teklu A, Barry C, Palumbo M, Weiwadel C, Kuthirummal N, Flagg J. Mechanical Characterization of Reduced Graphene Oxide Using AFM. Advances in Condensed Matter Physics. 2019. https://doi.org/10.1155/2019/8713965

[32] Rameli N, Jumbri K, Wahab RA, Ramli A, Huyop F. Synthesis and characterization of mesoporous silica nanoparticles using ionic liquids as a template. Journal of Physics: Conference Series. 2018; 1123:012068. https://doi.org/10.1088/1742-6596/1123/1/012068

[33] Parlak O, Turner APF, Tiwari A. PH-induced on/off-switchable graphene bioelectronics. Journal of Materials Chemistry B. 2015; 3:7434–7439. https://doi.org/10.1039/c5tb01355k

[34] Li D, Müller MB, Gilje S, Kaner RB, Wallace GG. Processable aqueous dispersions of graphene nanosheets. Nature Nanotechnology. 2008; 3:101–105. https://doi.org/10.1038/nnano.2007.451

[35] Mypati S, Sellathurai A, Kontopoulou M, Docoslis A, Barz DPJ. High concentration graphene nanoplatelet dispersions in water stabilized by graphene oxide. Carbon. 2021; 174:581–593. https://doi.org/10.1016/j.carbon.2020.12.068

[36] Han M, Xu B, Zhang M, Yao J, Li Q, Chen W, Zhou W. Preparation of biologically reduced graphene oxide-based aerogel and its application in dye adsorption. Science of The Total Environment. 2021; 783:147028. https://doi.org/10.1016/j.scitotenv.2021.147028

[37] Tajiki A;, Abdouss, Majid. Synthesis and Characterization of Graphene Oxide Nano-Sheets for Effective Removal of Copper Phthalocyanine from Aqueous Media. Iranian Journal of Chemistry and Chemical Engineering (IJCCE). 2017; 36:1–9. https://doi.org/10.30492/IJCCE.2017.28702

[38] Iqbal MZ, Abdala AA. Thermally reduced graphene: synthesis, characterization and dye removal applications. RSC Advances. 2013; 3:24455–64. https://doi.org/10.1039/C3RA43914C

[39] Uslu G, Tanyol M. Equilibrium and thermodynamic parameters of single and binary mixture biosorption of lead (II) and copper (II) ions onto Pseudomonas putida: Effect of temperature. Journal of Hazardous Materials. 2006; 135:87–93. https://doi.org/10.1016/J.JHAZMAT.2005.11.029

[40] Iqbal MZ, Abdala AA. Thermally reduced graphene: synthesis, characterization and dye removal applications. RSC Advances. 2013; 3:24455–64. https://doi.org/10.1039/C3RA43914C

[41] Al-Ghouti MA, Da'ana DA. Guidelines for the use and interpretation of adsorption isotherm models: A review. Journal of Hazardous Materials. 2020; 393:122383. https://doi.org/10.1016/J.JHAZMAT.2020.122383

[42] Nizam NUM, Hanafiah MM, Mahmoudi E, Halim AA, Mohammad AW. The removal of anionic and cationic dyes from an aqueous solution using biomass-based activated carbon. Scientific Reports. 2021; 11. https://doi.org/10.1038/s41598-021-88084-z

[43] Corda NC, Kini MS. A Review on Adsorption of Cationic Dyes using Activated Carbon. MATEC Web of Conferences. 2018; 144:02022. https://doi.org/10.1051/matecconf/201814402022

[44] Bensalah J, Habsaoui A, Dagdag O, Lebkiri A, Ismi I, Rifi EH, Warad I, Zarrouk A. Adsorption of a cationic dye (Safranin) by artificial cationic resins Amberlite®IRC-50: Equilibrium, kinetic and thermodynamic study. Chemical Data Collections. 2021; 35. https://doi.org/10.1016/j.cdc.2021.100756

[45] Goswami M, Phukan P. Enhanced adsorption of cationic dyes using sulfonic acid modified activated carbon. Journal of Environmental Chemical Engineering. 2017; 5:3508–3517. https://doi.org/10.1016/j.jece.2017.07.016

[46] Badawi AK, Abd Elkodous M, Ali GAM. Recent advances in dye and metal ion removal using efficient adsorbents and novel nano-based materials: An overview. RSC Advances. 2021; 11:36528–36553. https://doi.org/10.1039/d1ra06892j

[47] Kandil H, Ali H. Simultaneous Removal of Cationic Crystal Violet and Anionic Reactive Yellow Dyes using eco-friendly Chitosan Functionalized by Talc and Cloisite 30B. Journal of Polymers and the Environment. 2023; 31:1456–1477. https://doi.org/10.1007/s10924-022-02682-0